ELSEVIER

Applied Mathematical Modelling 24 (2000) 147–163

APPLIED MATHEMATICAL MODELLING

www.elsevier.nl/locate/apm

Modelling dynamics of piezoelectric solids in the two-dimensional case

R.V.N. Melnik [a,*], K.N. Melnik [b]

[a] *Department of Mathematics and Computing, University of Southern Queensland, Qld 4350, Australia*
[b] *Electronic Data Systems, 60 Waymouth Street, Adelaide 5000, Australia*

Received 6 January 1998; received in revised form 25 June 1999; accepted 29 July 1999

Abstract

This paper deals with the accuracy issues for a numerical scheme applied to coupled dynamic problems of electroelasticity. The computational results are discussed with examples for thin finite-dimension piezoceramic solids poled radially and circularly.

Keywords: Electro-mechanical interactions; Hollow piezoceramic cylinders; Corner points; Accuracy estimates

1. Introduction

In many applications, advanced structure design with integrated self-monitoring and control capabilities has become increasingly important. Due to the coupling phenomenon between electric and elastic fields, piezoelectric materials are widely used in such design as sensors, actuators, and transducers [5,17]. As a rapidly developing area of such utilisation we mention the integral incorporation of mechanical actuation and sensing microstructures into electronic chips [1,4]. Micro-electr-omechanical structures and piezoelectric semiconductors have features that may not be attained by purely electronic means. These new horizons of piezoelectric applications together with their traditional areas of application have stimulated a greater interest in rigorous mathematical approaches for the investigation of coupling phenomenon in piezoelectric materials.

This paper contributes to the subject of mathematical modelling of piezoelectric structures and deals with dynamic rather than steady-state problems for which coupling between electric and elastic fields may be substantial. We investigate a numerical procedure for the solution of such problems applied to thin finite-dimensional structures. In particular, we present computational results for thin hollow piezoceramic structures. These structures have become an important element of design in many technical devices and have potential for future applications [7,10]. They may also be used as a basis for further investigation of the piezoelectric effect in bones [8].

* Corresponding author. Present address: Mathematical Modelling of Industrial Processes, CSIRO Mathematical and Information Sciences, North Ryde (Sydney), NSW 1670, Australia. Tel.: +61-7-463-12632; fax: +61-7-463-11775.
E-mail address: melnik@usq.edu.au (R.V.N. Melnik).

0307-904X/00/$ - see front matter
PII: S0307-904X(99)00032-3

The trend towards miniaturisation of piezoelectric sensors and actuators leads to a situation where standard approaches based on thickness averaging (for mechanical components of electroelastic fields) and the use of Kirchoff-type hypotheses may not be appropriate. Under such circumstances the development of effective numerical methods becomes important in the investigation of both the statics and dynamics of coupled electroelastic fields [3,12–16,18–20,27]. For those applications that require smaller size and improved resolution of devices (for example, in biomedical imaging, nondestructive evaluation, etc.), thin structures produced from hollow spheres or cylinders may be good candidates to satisfy size and performance requirements [7].

The paper is organized as follows.

- Mechanical and mathematical notation is introduced in Section 2.
- Sections 3 and 4 provide the reader with the mathematical model and the numerical scheme for coupled problems of dynamic electroelasticity in the two-dimensional case.
- In Sections 5 and 6 we give the rigorous mathematical justification of the numerical method. Accuracy estimates are also derived in these sections.
- Section 7 describes the results of computational experiments conducted for finite-length piezoceramic cylinders poled radially and circularly.
- Conclusions are given in Section 8.

2. Notation

The following notations are used throughout this paper.

Mechanical notation:

- u_r and u_z are components of the displacement vector;
- $f_i,\ i = 1,2$ are components of the vector of mass forces;
- f_3 is the volume charge function;
- ρ is the density of the piezoceramic material;
- E_r and E_z are vector components of the stress of electric field;
- D_r and D_z are vector components of electric induction;
- c_{kl} are tensor components of elastic quantities;
- e_{ij} are tensor components of electro-elastic quantities;
- ϵ_{kl} are tensor components of electric quantities;

Mathematical notation:

- $\bar{Q}_T = \bar{G} \times \bar{I}$ is the space–time region of interest with $\bar{G} = \{(r,z):\ R_0 \leqslant r \leqslant R_1,\ Z_0 \leqslant z \leqslant Z_1\}$ (see Fig.1) and $\bar{I} = \{t:\ 0 \leqslant t \leqslant T\}$;
- $\gamma_1 = \{(r,z):\ R_0 < r < R_1, z = Z_0\},\ \gamma_2 = \{(r,z):\ R_0 < r < R_1, z = Z_1\},\ \gamma_3 = \{(r,z):\ r = R_0,\ Z_0 < z < Z_1\}$, $\gamma_4 = \{(r,z):\ r = R_1, Z_0 < z < Z_1\}$, are boundaries of the spatial region $\bar{G}$;
- $\gamma_{13} = \{r = R_0, z = Z_0\},\ \gamma_{23} = \{r = R_0, z = Z_1\},\ \gamma_{24} = \{r = R_1, z = Z_1\},\ \gamma_{14} = \{r = R_1, z = Z_0\}$ are corner points of $\bar{G}$;
- $\bar{\omega}_{h\tau} = \bar{\omega}_h \times \bar{\omega}_\tau$ is the discrete grid that covers the region $\bar{Q}_T$ with $\bar{\omega}_h = \bar{\omega}_{h_1} \times \bar{\omega}_{h_2}$, $\bar{\omega}_{h_1} = \{r_i:\ r_i = R_0 + ih_1, i = 0,1,\ldots,N, h_1 = (R_1 - R_0)/N\}$, $\bar{\omega}_{h_2} = \{z_j:\ z_j = Z_0 + jh_2, j = 0,1,\ldots,M, h_2 = (Z_1 - Z_0)/M\}$, and $\bar{\omega}_\tau = \{t_k:\ t_k = k\tau, \tau = T/L, k = 0,1,\ldots,L\}$;
- $\bar{r} = r - h_1/2, \bar{z} = z - h_2/2$ are "flux" nodes where deformations and stresses are defined;
- $\omega_{h_1} = \{r_i = R_0 + ih_1, i = 1,\ldots,N-1\},\ \omega^+_{h_1} = \{r_i = R_0 + ih_1, i = 1,\ldots,N\}$, and $\omega^-_{h_1} = \{r_i = R_0 + ih_1, i = 0,\ldots,N-1\}$ are auxiliary grids in the r-direction (analogously we define grids ω_{h_2}, $\omega^+_{h_2}$, $\omega^-_{h_2}$, ω_h, etc.);

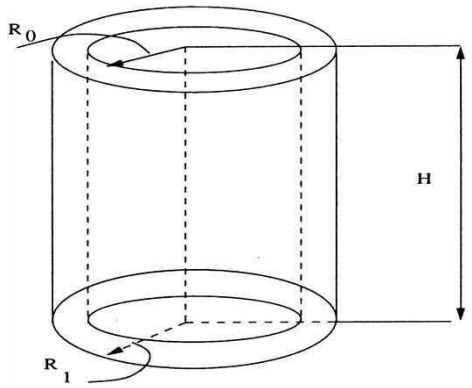

Fig. 1. Hollow piezoceramic cylinder ($l = R_1 - R_0,\ l/H < R_1/H = a$).

- if $y(r,z,t) \in \bar{\omega}_{h\tau}$ is a grid function, then $y_{\bar{r}}$, y_r, $y_{\dot{r}}$, and $y_{\bar{r}r}$ denote the first backward, forward, central and the second central difference derivatives in the r-direction, respectively (for difference derivatives in the z-direction and temporal difference derivatives we use analogous notation);
- other notation is explained in the text when appropriate.

3. Mathematical model

In order to describe the propagation process of electroelastic waves in hollow finite piezoceramic cylinders we use a coupled nonstationary system of partial differential equations which includes:

- the equation of motion of piezoelastic continuum media in cylindrical coordinates

$$\rho \frac{\partial^2 u_r}{\partial t^2} = \frac{\partial \sigma_r}{\partial r} + \frac{\partial \sigma_{rz}}{\partial z} + \frac{\sigma_r - \sigma_\theta}{r} + f_1, \tag{3.1}$$

$$\rho \frac{\partial^2 u_z}{\partial t^2} = \frac{\partial \sigma_{rz}}{\partial r} + \frac{\partial \sigma_z}{\partial z} + \frac{\sigma_{rz}}{r} + f_2, \tag{3.2}$$

- the Maxwell equation for piezoelectrics (in the acoustic range of frequencies, it is the forced electrostatic equation of dielectrics)

$$\frac{1}{r}\frac{\partial}{\partial r}(rD_r) + \frac{\partial D_z}{\partial z} = f_3, \tag{3.3}$$

- and state equations for piezoceramics with radial preliminary polarisation

$$\sigma_r = c_{33}\epsilon_r + c_{13}(\epsilon_\theta + \epsilon_z) - e_{33}E_r, \qquad \sigma_\theta = c_{13}\epsilon_r + c_{11}\epsilon_\theta + c_{12}\epsilon_z - e_{13}E_r, \tag{3.4}$$

$$\sigma_z = c_{13}\epsilon_r + c_{12}\epsilon_\theta + c_{11}\epsilon_z - e_{13}E_r, \qquad \sigma_{rz} = c_{44}\epsilon_{rz} - e_{15}E_z, \tag{3.5}$$

$$D_r = e_{33}\epsilon_r + e_{13}(\epsilon_\theta + \epsilon_z) + \epsilon_{33}E_r, \qquad D_z = 2e_{15}\epsilon_{rz} + \epsilon_{11}E_z \tag{3.6}$$

(the reader may consult, for example, [2,11] for similar expressions in the case of circular preliminary polarisation).

The relationship between deformations and displacements is of the Cauchy type

$$\epsilon_r = \frac{\partial u_r}{\partial r}, \quad \epsilon_\theta = \frac{u_r}{r}, \quad \epsilon_z = \frac{\partial u_z}{\partial z}, \quad \epsilon_{rz} = \frac{1}{2}\left(\frac{\partial u_r}{\partial z} + \frac{\partial u_z}{\partial r}\right) \tag{3.7}$$

and the function of electrostatic potential is introduced by formulae

$$E_r = -\frac{\partial \varphi}{\partial r}, \quad E_z = -\frac{\partial \varphi}{\partial z}. \tag{3.8}$$

The system (3.1)–(3.8) is considered in the space–time region $\bar{Q}_T$, and supplemented by the following initial conditions:

$$u_r(r,z,0) = u_r^{(0)}(r,z), \qquad \frac{\partial u_r(r,z,0)}{\partial t} = u_r^{(1)}(r,z), \tag{3.9}$$

$$u_z(r,z,0) = u_z^{(0)}(r,z), \qquad \frac{\partial u_z(r,z,0)}{\partial t} = u_z^{(1)}(r,z). \tag{3.10}$$

The boundary conditions for this problem are defined as follows:

- mechanical boundary conditions

$$\sigma_r(R_i,z,t) = p_r^{(i)}(z,t), \qquad \sigma_z(r,Z_i,t) = p_z^{(i)}(r,t), \tag{3.11}$$

$$\sigma_{rz}(R_i,z,t) = p_{zt}^{(i)}(z,t), \quad \sigma_{rz}(r,Z_i,t) = p_{rt}^{(i)}(r,t), \qquad i = 0,1; \tag{3.12}$$

- electric boundary conditions

$$\varphi(R_i,z,t) = 0, \quad D_z(r,Z_i,t) = 0, \qquad i = 0,1. \tag{3.13}$$

Finally, we assume non-negativity of the potential energy of deformation

$$\delta_1 \sum_{i=1}^{4} \xi_i^2 \leqslant c_{33}\xi_1^2 + c_{11}(\xi_2^2 + \xi_3^2) + 2c_{13}(\xi_2\xi_1 + \xi_3\xi_1) + 2c_{12}\xi_3\xi_2 + 2c_{44}\xi_4^2, \quad \delta_1 > 0. \tag{3.14}$$

The results on the existence and uniqueness of generalised solutions for the model (3.1)–(3.13) can be found in [19]. We also recall that the total inner energy described by the model (3.1)–(3.13) is the sum $\mathscr{E} = K + W + P$, where

$$K = \frac{\rho}{2}\int\int_G r\left\{\left(\frac{\partial u_r}{\partial t}\right)^2 + \left(\frac{\partial u_z}{\partial t}\right)^2\right\} \mathrm{d}G$$

is the kinetic energy of the system,

$$W = \frac{1}{2}\int\int_G r\left\{c_{33}\epsilon_r^2 + c_{11}(\epsilon_\theta^2 + \epsilon_z^2) + 2c_{13}(\epsilon_\theta\epsilon_r + \epsilon_z\epsilon_r) + 2c_{12}\epsilon_z\epsilon_\theta + 2c_{44}\epsilon_{rz}^2\right\} \mathrm{d}G$$

is the energy of elastic deformation, and

$$P = \frac{\epsilon_{33}}{2}\int\int_G rE_r^2 \,\mathrm{d}G + \frac{\epsilon_{11}}{2}\int\int_G rE_z^2 \,\mathrm{d}G$$

is the energy of the electric field.

It was shown in [22] that $\mathscr{E}$ satisfies the following energy balance equation:

$$\frac{\mathrm{d}\mathscr{E}}{\mathrm{d}t} = \int\int_G r\left[\frac{\partial D_r}{\partial t}E_r + \frac{\partial D_z}{\partial t}E_z\right]\mathrm{d}G + \int_{R_0}^{R_1} r\left[\sigma_{rz}\frac{\partial u_r}{\partial t} + \sigma_z\frac{\partial u_z}{\partial t}\right]\mathrm{d}r\Bigg|_{Z_0}^{Z_1} + \int_{Z_0}^{Z_1} r\left[\sigma_r\frac{\partial u_r}{\partial t} + \sigma_{rz}\frac{\partial u_z}{\partial t}\right]\mathrm{d}z\Bigg|_{R_0}^{R_1} + \int\int_G r\left[f_1\frac{\partial u_r}{\partial t} + f_2\frac{\partial u_z}{\partial t}\right]\mathrm{d}G. \tag{3.15}$$

Moreover, the functional $\mathscr{E}$ is bounded and the solution of (3.1)–(3.13) possesses the property given by the following theorem [22].

Theorem 3.1. *If the condition* (3.14) *is satisfied, the solution of the problem* (3.1)–(3.13) *is characterised by the following energy bound*:

$$\begin{aligned}\mathscr{E}(t_1) \leqslant M\Bigg\{ & \rho\int\int_G r\left[(u_r^{(1)})^2 + (u_z^{(1)})^2\right]\mathrm{d}G + \int\int_G r\left[c_{33}\epsilon_r^2 + c_{11}(\epsilon_\theta^2 + \epsilon_z^2)\right. \\ & \left. + 2c_{13}(\epsilon_\theta + \ + \epsilon_z)\epsilon_r + 2c_{12}\epsilon_z\epsilon_\theta + 2c_{44}\epsilon_{rz}^2\right]\big|_{t=0}\mathrm{d}G \\ & + \int_{R_0}^{R_1}\left[\sum_{i,j=0}^{1}\left(|p_{rt}^{(i)}(r,t_j)|^2 + |p_z^{(i)}(r,t_j)|^2\right)\right]\mathrm{d}r \\ & + \int_{Z_0}^{Z_1}\left[\sum_{i,j=0}^{1}\left(|p_r^{(i)}(z,t_j)|^2 + |p_{zt}^{(i)}(z,t_j)|^2\right)\right]\mathrm{d}z \\ & + \int_0^{t_1}\int_{R_0}^{R_1}\sum_{i=0}^{1}\left[\left(\frac{\partial p_{rt}^{(i)}}{\partial t}\right)^2 + \left(\frac{\partial p_z^{(i)}}{\partial t}\right)^2\right]\mathrm{d}r\,\mathrm{d}t \\ & + \int_0^{t_1}\int_{Z_0}^{Z_1}\sum_{i=0}^{1}\left[\left(\frac{\partial p_r^{(i)}}{\partial t}\right)^2 + \left(\frac{\partial p_{zt}^{(i)}}{\partial t}\right)^2\right]\mathrm{d}z\,\mathrm{d}t \\ & + \int\int_G r\lambda^2\big|_{t=0}\mathrm{d}G + \int_0^{t_1}\int\int_G r(f_1^2 + f_2^2)\,\mathrm{d}G\,\mathrm{d}t\Bigg\},\end{aligned}$$

where $\mathscr{E}(t)$ is the total inner energy of the electro-mechanical system at time t, and λ is defined by the relationships

$$\frac{\partial\lambda}{\partial r} + \frac{\partial\lambda}{\partial z} = f_3, \qquad \lambda(R_0,z,t) = \lambda(r,Z_0,t) = 0.$$

4. Numerical schemes

The numerical scheme for the solution of problem (3.1)–(3.13) was derived from (3.15) using the concept of generalised solutions [22]. The scheme has the following form:

$$\rho y_{\bar{t}t} = \Lambda_1(y,g,\mu) + F_1, \qquad \rho g_{\bar{t}t} = \Lambda_2(y,g,\mu) + F_2, \qquad \Lambda_3(y,g,\mu) = F_3, \tag{4.1}$$

where functions y, g and μ are fully discrete functions that give approximations to $u_r(r,z,t)$, $u_z(r,z,t)$ and $\varphi(r,z,t)$, respectively. The explicit form of the operators Λ_i and the right-hand sides from (4.1) are given in Appendix A.

The state equations (3.4)–(3.6) are approximated by

$$\bar{\sigma}_r = c_{33}\bar{\epsilon}_r + c_{13}(\bar{\epsilon}_\theta + \bar{\epsilon}_z) - e_{33}\bar{E}_r, \qquad \bar{\sigma}_\theta = c_{13}\bar{\epsilon}_r + c_{11}\bar{\epsilon}_\theta + c_{12}\bar{\epsilon}_z - e_{13}\bar{E}_r, \tag{4.2}$$

$$\bar{\sigma}_z = c_{13}\bar{\epsilon}_r + c_{12}\bar{\epsilon}_\theta + c_{11}\bar{\epsilon}_z - e_{13}\bar{E}_r, \qquad \bar{\sigma}_{rz} = c_{44}\bar{\epsilon}_{rz} - e_{15}\bar{E}_z, \tag{4.3}$$

$$\bar{D}_r = \epsilon_{33}\bar{E}_r + e_{33}\bar{\epsilon}_r + e_{13}(\bar{\epsilon}_\theta + \bar{\epsilon}_z), \qquad \bar{D}_z = \epsilon_{11}\bar{E}_z + 2e_{15}\bar{\epsilon}_{rz}, \tag{4.4}$$

where the expressions

$$\bar{E}_r = \frac{1}{2}\left(\mu_{\bar{r}} + \mu_{\bar{r}}^{(-1_z)}\right), \qquad \bar{E}_z = \frac{1}{2}\left(\mu_{\bar{z}} + \mu_{\bar{z}}^{(-1_r)}\right), \tag{4.5}$$

$$\bar{\epsilon}_r = \frac{1}{2}\left(y_{\bar{r}} + y_{\bar{r}}^{(-1_z)}\right), \qquad \bar{\epsilon}_\theta = \frac{1}{4\bar{r}}\left(y + y^{(-1_r)} + y^{(-1_z)} + y^{(-1,-1)}\right), \tag{4.6}$$

$$\bar{\epsilon}_z = \frac{1}{2}\left(g_{\bar{z}} + g_{\bar{z}}^{(-1_r)}\right), \qquad 2\bar{\epsilon}_{rz} = \frac{1}{2}\left(y_{\bar{z}} + y_{\bar{z}}^{(-1_r)} + g_{\bar{r}} + g_{\bar{r}}^{(-1_z)}\right) \tag{4.7}$$

give approximations to the Cauchy relations (3.7) and electrostatic potential formulae (3.8).

The approximation of time derivatives in the initial conditions (3.9), (3.10) is performed with the fictitious-time-layer technique [20,24,25]. For $t = 0$ we have:

$$y(r,z,0) = u_r^{(0)}(r,z), \qquad g(r,z,0) = u_z^{(0)}(r,z). \tag{4.8}$$

$$\rho y_t = \rho u_r^{(1)} + \frac{\tau}{2}(F_1 + \Lambda_1(y,g,\mu)), \tag{4.9}$$

$$\rho g_t = \rho u_z^{(1)} + \frac{\tau}{2}(F_2 + \Lambda_2(y,g,\mu)). \tag{4.10}$$

The discrete analogue of the total inner energy of the electro-mechanical system is [19,22]:

$$\begin{aligned}\bar{\mathscr{E}}(t) = \rho \sum_{\bar{\omega}_h} r\hbar_1\hbar_2(y_{\bar{t}}^2 + g_{\bar{t}}^2) + \sum_{\omega_h^+} \bar{r}h_1h_2\Big\{ & c_{33}\Phi(\bar{\epsilon}_r) + c_{11}\Big(\Phi(\bar{\epsilon}_\theta) + \Phi(\bar{\epsilon}_z)\Big) \\ & + c_{13}\Big[\bar{\epsilon}_r(\bar{\epsilon}_\theta + \bar{\epsilon}_z) + \check{\bar{\epsilon}}_r(\check{\bar{\epsilon}}_\theta + \check{\bar{\epsilon}}_z) - \tau^2(\bar{\epsilon}_r)_{\bar{t}}\Big((\bar{\epsilon}_\theta)_{\bar{t}} + (\bar{\epsilon}_z)_{\bar{t}}\Big)\Big] \\ & + c_{12}\Big[\bar{\epsilon}_z\bar{\epsilon}_\theta + \check{\bar{\epsilon}}_z\check{\bar{\epsilon}}_\theta - \tau^2(\bar{\epsilon}_z)_{\bar{t}}(\bar{\epsilon}_\theta)_{\bar{t}}\Big] + 2c_{44}\Phi(\bar{\epsilon}_{rz}) + \epsilon_{33}\Phi(\bar{E}_r) + \epsilon_{11}\Phi(\bar{E}_z)\Big\},\end{aligned} \tag{4.11}$$

where

$$\Phi(y) = \frac{(y + \check{y})^2}{4} - \frac{\tau^2}{4}(y_{\bar{t}})^2.$$

Then the stability conditions for the numerical scheme (4.1)–(4.10) follow from the non-negativity of (4.11) (see details in [23]):

$$
\begin{aligned}
&\frac{\tau^2}{h_1^2}c_1^2\left[\left(1+\frac{h_1}{2R_0}\right)\frac{1+K_1/\epsilon^M}{1+K_1}+\frac{c_{13}}{8c_{33}(1+K_1)}\frac{h_1}{h_2}+\frac{c_{13}h_1}{4R_0c_{33}(1+K_1)}+\frac{1}{4R_0^2c_{33}(1+K_1)}\left(c_{11}+\frac{e_{13}^2}{\epsilon_{33}\epsilon^M}\right)h_1^2\right]\\
&\quad+\frac{\tau^2}{h_2^2}c_2^2\left[\left(1+\frac{h_1}{2R_0}\right)\frac{1+2K_2/\epsilon^M}{1+K_2}+\frac{c_{13}}{8c_{44}(1+K_2)}\frac{h_2}{h_1}+\frac{c_{12}}{8R_0c_{44}(1+K_2)}h_2\right]\leqslant 1-\epsilon_1,\\
&\frac{\tau^2}{h_2^2}c_3^2\left[\left(1+\frac{h_1}{2R_0}\right)\frac{1+K_3/\epsilon^M}{1+K_3}+\frac{c_{13}}{8c_{11}(1+K_3)}\frac{h_2}{h_1}+\frac{c_{12}h_2}{8R_0c_{11}(1+K_1)}\right]\\
&\quad+\frac{\tau^2}{h_1^2}c_2^2\left[\left(1+\frac{h_1}{2R_0}\right)\frac{1+2K_2/\epsilon^M}{1+K_2}+\frac{c_{13}}{8c_{44}(1+K_2)}\frac{h_1}{h_2}\right]\leqslant 1-\epsilon_2,
\end{aligned}
\tag{4.12}
$$

where

$$
c_1=\sqrt{\frac{c_{33}(1+K_1)}{\rho}},\qquad c_2=\sqrt{\frac{c_{44}(1+K_2)}{\rho}},\qquad c_3=\sqrt{\frac{c_{11}(1+K_3)}{\rho}}
$$

are velocities of the three plane waves (quasi-longitudinal and two quasi-transverse) that, in the general case, propagate in an anisotropic electro-elastic medium (see [2,6]), and

$$
K_1=\frac{e_{33}^2}{\epsilon_{33}c_{33}},\quad K_2=\frac{e_{15}^2}{\epsilon_{11}c_{44}},\quad K_3=\frac{e_{13}^2}{\epsilon_{11}c_{11}}
$$

are constants of electro-mechanical coupling, $\epsilon^M=\min\{1/2,\epsilon_{11}/\epsilon_{33}\}$, and ϵ_i, $i=1,2$ are positive constants that do not depend on steps τ, h_1 and h_2.Finally, we recall (see [23] for details) that the solution of numerical model (4.1)–(4.10) is the subject of the discrete analogue of Theorem 3.1.

Theorem 4.1. *If conditions* (4.12) *are satisfied then the solution of the discrete model* (4.1)–(4.10) *satisfies the following estimate*:

$$
\begin{aligned}
\bar{\mathscr{E}}(t_1+\tau)\leqslant M\Bigg\{&\rho\sum_{\bar{\omega}_h}r\hbar_1\hbar_2\Big((y_t(0))^2+(g_t(0))^2\Big)+\sum_{\omega_h^+}\bar{r}h_1h_2\Bigg\{c_{33}\left[(\bar{\epsilon}_r(0))^2+\frac{\tau^2}{4}((\bar{\epsilon}_r(0))_t)^2\right]\\
&+c_{11}\left[(\bar{\epsilon}_\theta(0))^2+(\bar{\epsilon}_z(0))^2+\frac{\tau^2}{4}\Big(((\bar{\epsilon}_\theta(0))_t)^2+((\bar{\epsilon}_z(0))_t)^2\Big)\right]\\
&+c_{13}\Bigg[\bar{\epsilon}_r(0)\Big(\bar{\epsilon}_\theta(0)+\bar{\epsilon}_z(0)\Big)+\frac{\tau}{2}\Big(\bar{\epsilon}_r(0)\Big((\bar{\epsilon}_\theta(0))_t+(\bar{\epsilon}_z(0))_t\Big)\\
&+(\bar{\epsilon}_r(0))_t\Big(\bar{\epsilon}_\theta(0)+\bar{\epsilon}_z(0)\Big)\Big)\Bigg]+c_{12}\Big[\bar{\epsilon}_z(0)\bar{\epsilon}_\theta(0)+\frac{\tau}{2}\Big(\bar{\epsilon}_z(0)(\bar{\epsilon}_\theta(0))_t+(\bar{\epsilon}_z(0))_t\bar{\epsilon}_\theta(0)\Big)\Big]\\
&+2c_{44}\left[(\bar{\epsilon}_{rz}(0))^2+\frac{\tau^2}{4}((\bar{\epsilon}_{rz}(0))_t)^2\right]\Bigg\}+\sum_{\bar{\omega}_{h_1}}r\hbar_1\max_{0,\tau,t_1,t_1+\tau}\left[\sum_{k=0}^{1}\Big((p_z^{(k)})^2+(p_{rt}^{(k)})^2\Big)\right]\\
&+\sum_{\bar{\omega}_{h_2}}r\hbar_2\max_{0,\tau,t_1,t_1+\tau}\left[\sum_{k=0}^{1}\Big((p_r^{(k)})^2+(p_{rz}^{(k)})^2\Big)\right]\\
&+\sum_{t'=\tau}^{t_1}\left\{\sum_{\bar{\omega}_{h_1}}r\hbar_1\left[\sum_{k=0}^{1}\Big(|(p_z^{(k)})_{\bar{t}}|^2+|(p_{rt}^{(k)})_{\bar{t}}|^2\Big)\right]\right.
\end{aligned}
$$

$$+\sum_{\bar{\omega}_{h_2}} r\hbar_2\left[\sum_{k=0}^{1}\left(|(p_r^{(k)})_{\check{t}}|^2+|(p_{rz}^{(k)})_{\check{t}}|^2\right)\right]\Bigg\}$$

$$+\sum_{\omega_h^+}\bar{r}h_1h_2(\bar{\lambda}(0))^2+\sum_{t'=\tau}^{t_1}\tau\sum_{\bar{\omega}_h} r\hbar_1\hbar_2(f_1^2+f_2^2)\Bigg\}, \tag{4.13}$$

with the discrete energy function defined by (4.11) *and the function* $\bar{\lambda}$ *defined by the following relationships*:

$$\left(\bar{r}\frac{\bar{\lambda}+\bar{\lambda}^{(+1_z)}}{2}\right)_r+\left(\frac{\bar{r}\bar{\lambda}+\bar{r}^{(+1)}\bar{\lambda}^{(+1_r)}}{2}\right)_z=rf_3, \tag{4.14}$$

$$\bar{\lambda}^{(+1_r)}=\bar{D}_r^{(+1_r)} \quad \textit{for } r=R_0, \quad \textit{and} \quad \bar{\lambda}^{(+1_z)}=\bar{D}_z^{(+1_z)} \quad \textit{for } z=Z_0 \ \ \forall t\in\bar{\omega}_\tau. \tag{4.15}$$

5. Convergence of discrete approximations and accuracy of numerical schemes

The error of the scheme (4.1)–(4.10),

$$z_1=y-u_r, \quad z_2=g-u_z, \quad \zeta=\mu-\varphi, \tag{5.1}$$

can be defined as the solution of the following operator-difference scheme:

$$\begin{aligned}
&\rho(z_1)_{\bar{t}t}=\Lambda_1(z_1,z_2,\zeta)+\psi_1, && t\in\omega_\tau,\\
&\rho(z_2)_{\bar{t}t}=\Lambda_2(z_1,z_2,\zeta)+\psi_2, && t\in\omega_\tau,\\
&\Lambda_3(z_1,z_2,\zeta)=\psi_3, && t\in\bar{\omega}_\tau,
\end{aligned} \tag{5.2}$$

with the initial conditions

$$z_i=0, \quad \rho(z_i)_t=\psi_i, \qquad i=1,2 \quad \text{when } t=0. \tag{5.3}$$

The right-hand sides in (5.2), (5.3) are defined as follows:

$$\psi_1=\begin{cases}-\rho(u_r)_{\bar{t}t}+(F_1-\Lambda_1(u_r,u_z,\varphi)) & \text{for } t\in\omega_\tau,\\ \rho u_r^{(1)}-\rho(u_r)_t+(\tau/2)(F_1-\Lambda_1(u_r,u_z,\varphi)) & \text{for } t=0,\end{cases} \tag{5.4}$$

$$\psi_2=\begin{cases}-\rho(u_z)_{\bar{t}t}+(F_2-\Lambda_2(u_r,u_z,\varphi)) & \text{for } t\in\omega_\tau,\\ \rho u_z^{(1)}-\rho(u_z)_t+(\tau/2)(F_2-\Lambda_2(u_r,u_z,\varphi)) & \text{for } t=0,\end{cases} \tag{5.5}$$

$$\psi_3=F_3-\Lambda_3(u_r,u_z,\varphi) \quad \text{for } t\in\bar{\omega}_\tau. \tag{5.6}$$

As in the one-dimensional case [20], it can be shown that if the solution of (3.1)–(3.13) belongs to the Sobolev class $(W_2^4(Q_T))^2\times L_2(I,W_2^4(G))$, then the approximation errors $\psi_i, i=1,2,3$ defined by (5.4)–(5.6) can be represented in the form

$$\psi_i=\breve{\psi}_i+\delta_1(h_1)\overset{*}{\psi}_i+\delta_2(h_2)\overset{**}{\psi}_i, \quad i=1,2, \qquad \psi_3=\breve{\psi}_3+\delta_3(h_2)\overset{**}{\psi}_3 \tag{5.7}$$

for any $t \in \bar{\omega}_\tau$, where

$$\delta_1(h_1) = \begin{cases} 0, & \omega_h \cup \gamma_1 \cup \gamma_2, \\ -2/h_1, & \bar{\gamma}_3, \\ 2/h_1, & \bar{\gamma}_4, \end{cases} \qquad \delta_2(h_2) = \begin{cases} 0, & \omega_h \cup \gamma_3 \cup \gamma_4, \\ -2/h_2, & \bar{\gamma}_1, \\ 2/h_2, & \bar{\gamma}_2, \end{cases}$$

$$\delta_3(h_2) = \begin{cases} 0, & \omega_h \cup \bar{\gamma}_3 \cup \bar{\gamma}_4, \\ -2/h_2, & \gamma_1, \\ 2/h_2, & \gamma_2, \end{cases}$$

$$\breve{\psi}_i = \mathrm{O}(|h|^2 + \tau^2) \ \ \forall (r,z) \in \bar{\omega}_h, \quad |h|^2 = h_1^2 + h_2^2, \ \ i = 1,2, \quad \breve{\psi}_3 = \mathrm{O}(|h|^2), \tag{5.8}$$

and the functionals $\overset{*}{\psi}_i, i = 1,2, \overset{**}{\psi}_j, j = 1,2,3$ have the second order of smallness with respect to $|h|$ except at corner points. In the corner points we have

$$\overset{*}{\psi}_i = \mathrm{O}(h_2 + h_1^2), \ \ i = 1,2, \quad \overset{**}{\psi}_j = \mathrm{O}(h_1 + h_2^2), \ \ j = 1,2,3. \tag{5.9}$$

Assuming that the stability conditions (4.12) are satisfied from (4.13) (Theorem 4.1) we obtain the following accuracy estimate for our numerical method:

$$\begin{aligned} \breve{\mathscr{E}}(t_1 + \tau) \leqslant M \Bigg\{ & \sum_{\omega_h} r h_1 h_2 \Big((\breve{\psi}_1(r,z,0))^2 + (\breve{\psi}_2(r,z,0))^2 \Big) \\ & + \sum_{\omega^+} \bar{r} h_1 h_2 \Big\{ c_{33} (\breve{\epsilon}_r(0))^2 + c_{11} \Big((\breve{\epsilon}_\theta(0))^2 + (\breve{\epsilon}_z(0))^2 \Big) \\ & + c_{13} \Big[\breve{\epsilon}_r(0) \Big(\breve{\epsilon}_\theta(0) + \breve{\epsilon}_z(0) \Big) \Big] + c_{12} \breve{\epsilon}_z(0) \breve{\epsilon}_\theta(0) + 2 c_{44} (\breve{\epsilon}_{rz}(0))^2 \Big\} \\ & + \sum_{\bar{\omega}_1} r \hbar_1 \max_{0,\tau,t_1,t_1+\tau} \Big((\overset{**}{\psi}_1)^2 + (\overset{**}{\psi}_2)^2 \Big) + \sum_{\bar{\omega}_2} r \hbar_2 \max_{0,\tau,t_1,t_1+\tau} \Big((\overset{*}{\psi}_1)^2 + (\overset{*}{\psi}_2)^2 \Big) \\ & + \sum_{t'=\tau}^{t_1} \tau \Bigg\{ \sum_{\bar{\omega}_{h_1}} r \hbar_1 \Big(((\overset{**}{\psi}_1)_{\breve{t}})^2 + \Big((\overset{**}{\psi}_2)_{\breve{t}} \Big)^2 \Big) + \sum_{\bar{\omega}_{h_2}} r \hbar_2 \Big(\Big(\Big(\overset{*}{\psi}_1 \Big)_{\breve{t}} \Big)^2 + \Big(\Big(\overset{*}{\psi}_2 \Big)_{\breve{t}} \Big)^2 \Big) \Bigg\} \\ & + \sum_{t'=\tau}^{t_1} \tau \sum_{\omega_h} r h_1 h_2 \Big(\Big(\breve{\psi}_1 \Big)^2 + \Big(\breve{\psi}_2 \Big)^2 \Big) + \sum_{\omega_h^+} \bar{r} h_1 h_2 (\kappa(0))^2 \Bigg\}, \end{aligned} \tag{5.10}$$

where functions $\breve{\epsilon}_r$, $\breve{\epsilon}_\theta$, $\breve{\epsilon}_z$, $\breve{\epsilon}_{rz}$ in the right-hand side of (5.10) and the function $\breve{\mathscr{E}}$ are obtained from the corresponding functions $\bar{\epsilon}_r$, $\bar{\epsilon}_\theta$, $\bar{\epsilon}_z$, $\bar{\epsilon}_{rz}$ and $\bar{\mathscr{E}}$ by the change of y for z_1, g for z_2, and φ for ζ. Finally, the function κ in (5.10) is defined by the following relationships:

$$r\psi_3 = \left(\bar{r} \frac{\kappa + \kappa^{(+1_z)}}{2} \right)_r + \left(\frac{\bar{r}\kappa + \bar{r}^{(+1_r)} \kappa^{(+1_r)}}{2} \right)_z, \tag{5.11}$$

$$\kappa^{(+1_r)} = \overset{*}{D}_r^{(+1_r)} \quad \text{for } r = R_0, \qquad \kappa^{(+1_z)} = \overset{*}{D}_z^{(+1_z)} \quad \text{for } r = Z_0, \tag{5.12}$$

where $\overset{*}{D}_r$ and $\overset{*}{D}_z$ are obtained from $\bar{D}_r$ and $\bar{D}_z$ by the change of y for u_r, g for u_z, and μ for φ.

Hence, taking into account representations (5.7)–(5.9) the following result follows immediately from the estimate (5.10).

Theorem 5.1. *If stability conditions* (4.12) *are satisfied, then the solution of* (4.1)–(4.10) *converges in the energy norm to the solution of the differential problem* (3.1)–(3.13) *from the class* $(W_2^4(Q_T))^2 \times L_2(I, W_2^4(G))$ *with the speed* $\mathrm{O}(h_1^{3/2} + h_2^{3/2} + \tau^2)$. *The accuracy estimate* (5.10) *holds for any* $t_1 > 0$.

6. The improvement of approximations at corner points

Compared to the one-dimensional case [20], Theorem 5.1 gives us a weaker result due to the loss of half-order in the convergence speed. We note that the decrease in the order of spatial approximations is caused by the approximations of the mechanical boundary conditions in corner points. Similar difficulties arise even in the classical elasticity theory when, for example, on the one side of a rectangular plate we are given stresses, whereas on the adjoint side we are given one component of stress and one component of displacement.

An effective technique for the improvement of approximations at the corner points for mechanical boundary conditions in coupled problems of electroelasticity was proposed in [19]. It can be shown (for example, by using the Taylor's formula with the remainder in the integral form) that for the solution (u_r, u_z, φ) from $(W_2^4(Q_T))^2 \times L_2(I, W_2^4(G))$ we have

$$\psi_1 = \begin{cases} \dfrac{h_2}{h_1}\dfrac{\partial \sigma_r}{\partial z} + \dfrac{h_1}{h_2}\dfrac{1}{r}\dfrac{\partial}{\partial r}(r\sigma_{rz}) + \mathrm{O}(|h|^2 + \tau^2), & \text{when } (r,z) \in \gamma_{13} \cup \gamma_{24}, \\ -\dfrac{h_1}{h_2}\dfrac{1}{r}\dfrac{\partial}{\partial r}(r\sigma_{rz}) - \dfrac{h_2}{h_1}\dfrac{\partial \sigma_r}{\partial z} + \mathrm{O}(|h|^2 + \tau^2), & \text{when } (r,z) \in \gamma_{23} \cup \gamma_{14}, \end{cases} \tag{6.1}$$

$$\psi_2 = \begin{cases} \dfrac{h_1}{h_2}\dfrac{1}{r}\dfrac{\partial}{\partial r}(r\sigma_z) + \dfrac{h_2}{h_1}\dfrac{\partial \sigma_{rz}}{\partial z} + \mathrm{O}(|h|^2 + \tau^2), & \text{when } (r,z) \in \gamma_{13} \cup \gamma_{24}, \\ -\dfrac{h_2}{h_1}\dfrac{\partial \sigma_{rz}}{\partial z} - \dfrac{h_1}{h_2}\dfrac{1}{r}\dfrac{\partial}{\partial r}(r\sigma_z) + \mathrm{O}(|h|^2 + \tau^2), & \text{when } (r,z) \in \gamma_{23} \cup \gamma_{14}. \end{cases} \tag{6.2}$$

Then taking into account the conditions (3.11), (3.12) we set

$$F_1^c = \begin{cases} F_1, & \omega_h \cup \gamma_1 \cup \gamma_2 \cup \gamma_3 \cup \gamma_4, \\ f_1 - \dfrac{2}{h_1}p_r^{(0)} - \dfrac{2}{h_2}p_{rt}^{(0)} - \dfrac{h_2}{h_1}\dfrac{\partial p_r^{(0)}}{\partial z} - \dfrac{h_1}{h_2}\dfrac{1}{r}\dfrac{\partial}{\partial r}(rp_{rt}^{(0)}), & \gamma_{13}, \\ f_1 + \dfrac{2}{h_2}p_{rt}^{(1)} - \dfrac{2}{h_1}p_r^{(0)} + \dfrac{h_1}{h_2}\dfrac{1}{r}\dfrac{\partial}{\partial r}(rp_{rt}^{(1)}) + \dfrac{h_2}{h_1}\dfrac{\partial p_r^{(0)}}{\partial z}, & \gamma_{23}, \\ f_1 - \dfrac{2}{h_2}p_{rt}^{(0)} + \dfrac{2}{h_1}p_r^{(1)} + \dfrac{h_1}{h_2}\dfrac{1}{r}\dfrac{\partial}{\partial r}(rp_{rt}^{(0)}) + \dfrac{h_2}{h_1}\dfrac{\partial p_r^{(1)}}{\partial z}, & \gamma_{14}, \\ f_1 + \dfrac{2}{h_2}p_{rt}^{(1)} + \dfrac{2}{h_1}p_r^{(1)} - \dfrac{h_1}{h_2}\dfrac{1}{r}\dfrac{\partial}{\partial r}(rp_{rt}^{(1)}) - \dfrac{h_2}{h_1}\dfrac{\partial p_r^{(1)}}{\partial z}, & \gamma_{24}, \end{cases} \tag{6.3}$$

$$F_2^c = \begin{cases} F_2, & \omega_h \cup \gamma_1 \cup \gamma_2 \cup \gamma_3 \cup \gamma_4, \\ f_2 - \dfrac{2}{h_2} p_z^{(0)} - \dfrac{2}{h_1} p_{zt}^{(0)} - \dfrac{h_1}{h_2} \dfrac{1}{r} \dfrac{\partial}{\partial r}(r p_z^{(0)}) - \dfrac{h_2}{h_1} \dfrac{\partial p_{zt}^{(0)}}{\partial z}, & \gamma_{13}, \\ f_2 + \dfrac{2}{h_2} p_z^{(1)} - \dfrac{2}{h_1} p_{zt}^{(0)} + \dfrac{h_1}{h_2} \dfrac{1}{r} \dfrac{\partial}{\partial r}(r p_z^{(1)}) + \dfrac{h_2}{h_1} \dfrac{\partial p_{zt}^{(0)}}{\partial z}, & \gamma_{23}, \\ f_2 - \dfrac{2}{h_2} p_z^{(0)} + \dfrac{2}{h_1} p_{zt}^{(1)} + \dfrac{h_1}{h_2} \dfrac{1}{r} \dfrac{\partial}{\partial r}(r p_z^{(0)}) + \dfrac{h_2}{h_1} \dfrac{\partial p_{zt}^{(1)}}{\partial z}, & \gamma_{14}, \\ f_2 + \dfrac{2}{h_2} p_z^{(1)} + \dfrac{2}{h_1} p_{zt}^{(1)} - \dfrac{h_1}{h_2} \dfrac{1}{r} \dfrac{\partial}{\partial r}(r p_z^{(1)}) - \dfrac{h_2}{h_1} \dfrac{\partial p_{zt}^{(1)}}{\partial z}, & \gamma_{24}, \end{cases} \tag{6.4}$$

and consider a new numerical scheme

$$\rho y_{\bar{t}t} = \Lambda_1(y, g, \mu) + F_1^c, \qquad \rho g_{\bar{t}t} = \Lambda_2(y, g, \mu) + F_2^c, \qquad \Lambda_3(y, g, \mu) = F_3, \tag{6.5}$$

with F_1^c, F_2^c defined by (6.3), (6.4), and the following initial conditions:

$$\rho y_t = \rho u_r^{(1)} + (\tau/2)\big(F_1^c + \Lambda_1(y, g, \mu)\big), \qquad \rho g_t = \rho u_z^{(1)} + (\tau/2)\big(F_2^c + \Lambda_1(y, g, \mu)\big). \tag{6.6}$$

Approximations of state equations, Cauchy relations and those initial conditions not involving derivatives have the forms (4.2)–(4.8).

The error approximation of the numerical scheme (6.5), (6.6), (4.2)–(4.8) can be represented in the form analogous to (5.7), namely

$$\psi_i^c = \breve{\psi}_i^c + \delta_1(h_1)\overset{*}{\psi}_i^c + \delta_2(h_2)\overset{**}{\psi}_i^c, \quad i = 1, 2. \tag{6.7}$$

However, in the latter case if the solution of (3.1)–(3.13) belongs to the class $(W_2^4(Q_T))^2 \times L_2(I, W_2^4(G))$ all functionals $\breve{\psi}_i^c$, $\overset{**}{\psi}_i^c$, $\overset{**}{\psi}_i^c$ have the second order of smallness with respect to $|h|$.

As a result we have proved the following theorem:

Theorem 6.1. *The solution of the numerical scheme* (6.5), (6.6), (4.2)–(4.8) *converges to the solution of the differential problem* (3.1)–(3.13) *from the class* $(W_2^4(Q_T))^2 \times L_2(I, W_2^4(G))$ *in the energy norm with the second order accuracy with respect to space–time discretisation subject to the stability conditions* (4.12). *The accuracy estimate analogous to* (5.10) *holds for any* $t_1 > 0$ *with the change of functionals* $\breve{\psi}_i$, $\overset{*}{\psi}_i$, $\overset{**}{\psi}_i$ $(i = 1, 2)$ *for* $\breve{\psi}_i^c$, $\overset{**}{\psi}_i^c$, $\overset{**}{\psi}_i^c$, *respectively*.

7. Computational experiments

In this section we consider results for modelling piezoceramic solids under nonstationary conditions. As in [20], the main emphasis is the dynamics of radial displacements on the external surface of cylinders.

Eqs. (3.1), (3.2) are scaled to the following form:

$$\frac{\partial^2 u_r}{\partial t^2} = \frac{\partial \sigma_r}{\partial r} + a\frac{\partial \sigma_{rz}}{\partial z} + \frac{\sigma_r - \sigma_\Theta}{r} + f_1,$$

$$\frac{\partial^2 u_z}{\partial t^2} = \frac{\partial \sigma_{rz}}{\partial r} + a\frac{\partial \sigma_z}{\partial z} + \frac{\sigma_{rz}}{r} + f_2,$$

where a is the parameter that characterises the ratio of the cylinder thickness to its length (see Fig. 1).

The Maxwell equation (3.3) is transformed to the form

$$\frac{\epsilon_{33}}{\epsilon_{11}}\frac{1}{r}\frac{\partial}{\partial r}\left(r\frac{\partial\varphi}{\partial r}\right)+\frac{\partial^2\varphi}{\partial z^2}=F,$$

with

$$F=-\frac{f_3}{\epsilon_{11}}+\frac{1}{\epsilon_{11}}\frac{1}{r}\frac{\partial}{\partial r}[r(e_{33}\epsilon_r+e_{13}(\epsilon_\Theta+\epsilon_z))].$$

In all computations we assume that solids are made from PZT-piezoceramic materials for which scaled piezoelectric characteristics are as follows:

$$c_{11}=1,\quad c_{12}=0.559712,\quad c_{13}=0.534532,\quad c_{33}=0.827338,\quad c_{44}=0.220144,$$
$$e_{13}=-0.18605,\quad e_{33}=0.54027,\quad e_{15}=0.454383,\quad \epsilon_{11}=0.87,\quad \epsilon_{33}=1.$$

Mechanical boundary conditions follow from the assumption of zero stress on the interior and exterior surfaces. Initially, piezoceramic is assumed to be unexcited. The given potential difference ($2V=1$) is maintained between interior and exterior surfaces of the cylinders

$$\varphi=\pm 0.5,\quad r=R_0,R_1\quad\text{and}\quad\frac{\partial\varphi}{\partial z}=\frac{2e_{15}}{\epsilon_{11}}\epsilon_{rz},\quad z=Z_0,Z_1.$$

Computation has been conducted using the improved scheme (6.5),(6.6), (4.2)–(4.8). For the solution of the Maxwell equation we use the package ALTPACK which implements the alternating-triangular method [24,25].

Results obtained with the two-dimensional model for cylinders with small values of a (typically for $a=0.001$) practically coincide with the results obtained earlier for infinite-length cylinders with the one-dimensional model [20]. Therefore, in such situations the use of two-dimensional models is unnecessary and it is reasonable to confine themselves to the one-dimensional model.

For finite-length cylinders the situation is different. The analysis of radial displacements in time on the external surface shows that with the decrease in cylinder thickness the amplitude of oscillations increases for both types of cylinders [21], poled radially and circularly (see Fig. 2). However, the increase in amplitude for cylinders poled radially takes place much quicker. For small-thickness cylinders the amplitude of oscillations attains considerable values, many times

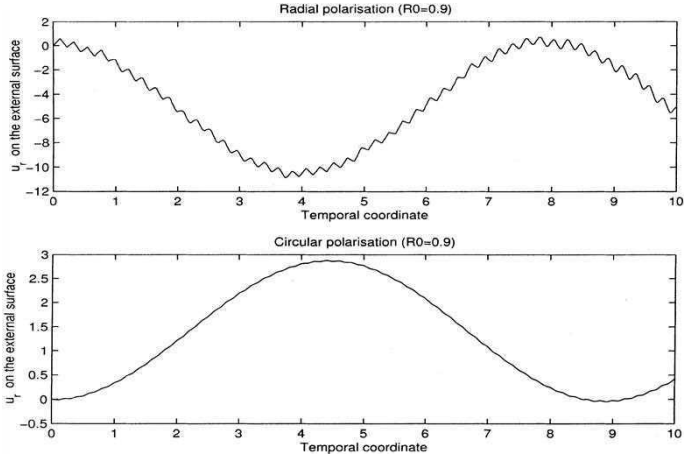

Fig. 2. Time dependency of radial displacements on the external surface of the piezoceramic cylinder ($l=0.1$, $a=1$).

greater than for cylinders poled circularly. This fact is a consequence of the strong coupling of elastic and electric fields in the case of radial polarisation compared to a weak coupling for cylinders poled circularly. Therefore, in general, for modelling finite-length piezoceramic cylinders it is essential to use two-dimensional models for cylinders poled both radially and circularly. We also note that compared to circular-poled cylinders, the error obtained with the one-dimensional model for cylinders poled radially could be considerably greater. Figs. 3 and 4 show the evolution of the radial displacements for finite-length cylinders with radial preliminary polarisation. In Figs. 5 and 6 we present the same characteristics for cylinders poled circularly.

In the design of various technical devices based on hollow piezoceramic cylinders, radiating properties of the external surface may essentially influence the overall device performance. If the radiation from the external surface of thin hollow piezoceramic cylinders has to be increased then

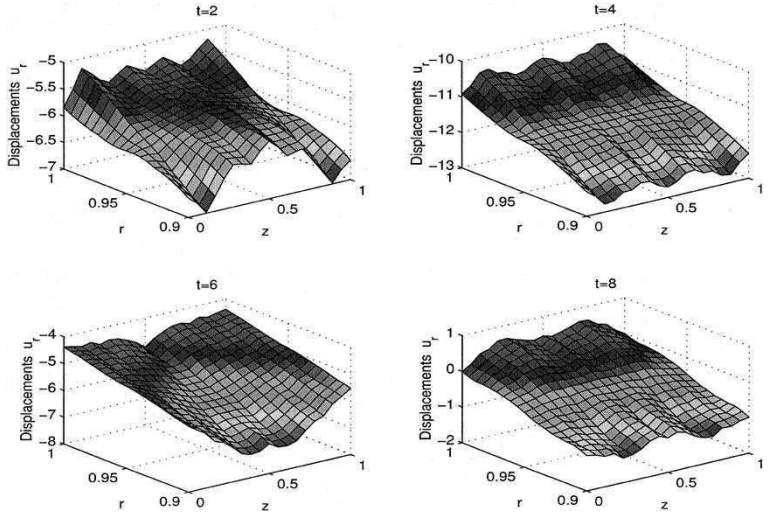

Fig. 3. Dynamics of radial displacements in the thin PZT-cylinder poled radially ($l = 0.1$, $a = 1$).

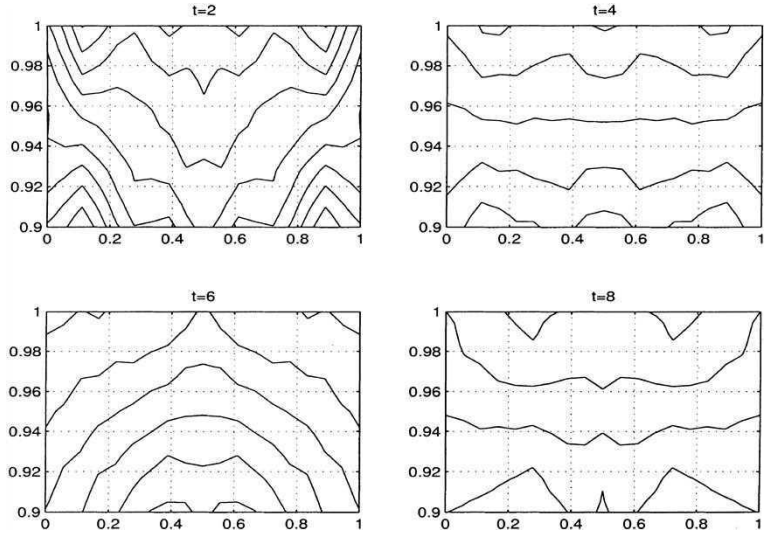

Fig. 4. Level curves of radial displacements in the thin piezoceramic cylinder poled radially ($l = 0.1$, $a = 1$).

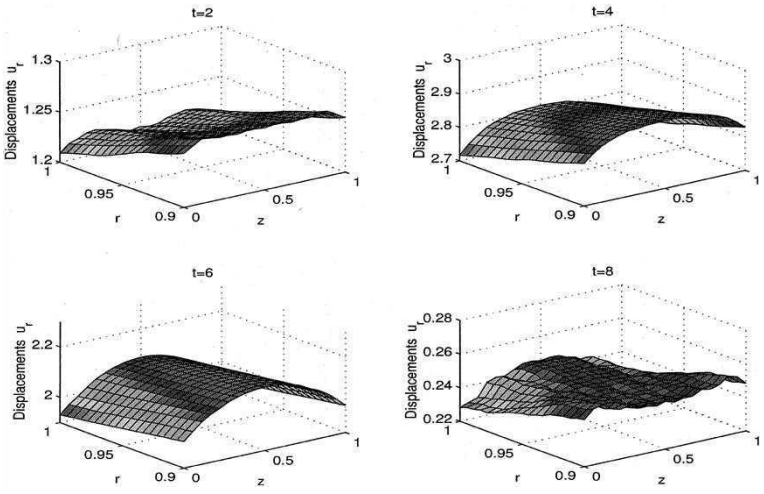

Fig. 5. Dynamics of radial displacements in the thin PZT-cylinders poled circularly ($l = 0.1$, $a = 1$).

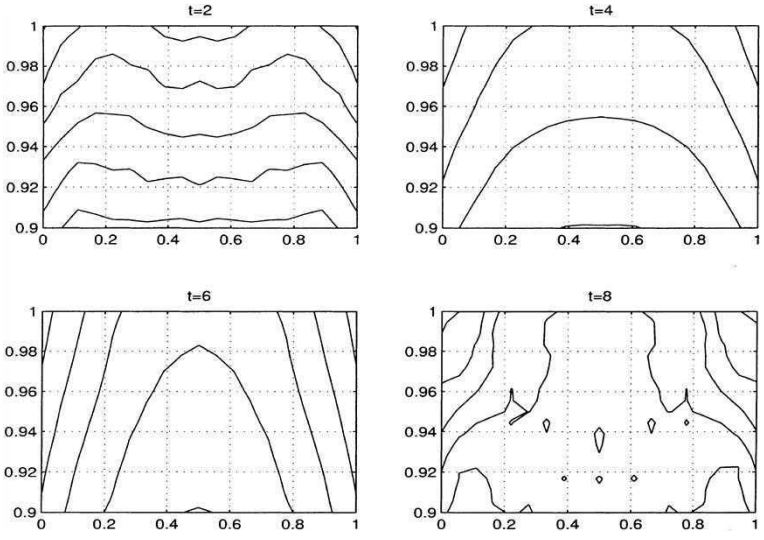

Fig. 6. Level curves of radial displacements in the thin piezoceramic cylinder poled circularly ($l = 0.1$, $a = 1$).

such cylinders have to be poled radially. In contrast, for thick hollow piezoceramic cylinders circular preliminary polarisation will lead to an increase in the degree of radiation from the external surface.

8. Conclusions and future directions

The question of accuracy is one of the most important issues in the theory and practice of approximate methods. In this paper we proved the accuracy theorems for an effective numerical method designed for the solution of a quite general class of coupled problems in dynamic theory of electroelasticity. Using numerical examples we demonstrated that taking into account the

coupling of elastic and electric fields, as well as anisotropy of physical properties of piezoelectric materials may essentially influence the quality of description of wave phenomena in piezoelectric solids.

An important direction in the future development of effective numerical procedures in coupled electroelasticity is connected with a wider application of piezocomposite materials. With piezoelectric material alone it is often difficult to simultaneously satisfy such requirements as broad operation frequency bandwidth, media adjustable acoustic impedance, and a high electro-mechanical coupling [9]. In such situations the use of piezoceramic-polymer composites may be advantageous. In some cases models in this field should incorporate such important effects as nonlocal memory effects, aging, interaction of coupled electroelastic fields with magnetic and thermal fields. This requires taking into account dissipations that may have different origins. The technique based on the Bloch expansion (see [26] and references therein) may prove to be useful in such situations.

Acknowledgements

This work was partially supported by grant USQ-PTRP 17989 and by Australian Research Council Grant 179406. The authors are grateful to Dr. David Smith and Tim Passmore for their suggestions of improvement and helpful assistance at the final stage of preparation of this paper.

Appendix A

The difference operators Λ_i and right-hand sides $F_i, i = 1,2,3$ in (5.2)–(5.5), (6.3)–(6.6) are defined as follows:

$$\Lambda_1(y,g,\mu) = \begin{cases} \frac{1}{r}\left(\bar{r}\frac{\bar{\sigma}_r+\bar{\sigma}_r^{(+1z)}}{2}\right)_r + \frac{1}{r}\left(\frac{\bar{r}\bar{\sigma}_{rz}+\bar{r}^{(+1)}\bar{\sigma}_{rz}^{(+1r)}}{2}\right)_z - \frac{\bar{\sigma}_\theta+\bar{\sigma}_\theta^{(+1r)}+\bar{\sigma}_\theta^{(+1z)}+\bar{\sigma}_\theta^{(+1,+1)}}{4r}, & (r,z)\in\omega_h,\\ \frac{1}{r}\left(\bar{r}\bar{\sigma}_r^{(+1z)}\right)_r + \frac{1}{r}\frac{2}{h_2}\left(\frac{\bar{r}\bar{\sigma}_{rz}^{(+1z)}+\bar{r}^{(+1)}\bar{\sigma}_{rz}^{(+1,+1)}}{2}\right) - \frac{\bar{\sigma}_\theta^{(+1z)}+\bar{\sigma}_\theta^{(+1,+1)}}{2r}, & (r,z)\in\gamma_1,\\ \frac{1}{r}\left(\bar{r}\bar{\sigma}_r\right)_r - \frac{1}{r}\frac{2}{h_2}\left(\frac{\bar{r}\bar{\sigma}_{rz}+\bar{r}^{(+1)}\bar{\sigma}_{rz}^{(+1r)}}{2}\right) - \frac{\bar{\sigma}_\theta+\bar{\sigma}_\theta^{(+1r)}}{2r}, & (r,z)\in\gamma_2,\\ \frac{1}{r}\bar{r}^{(+1)}\left(\bar{\sigma}_{rz}^{(+1r)}\right)_z + \frac{1}{r}\frac{2}{h_1}\bar{r}^{(+1)}\left(\frac{\bar{\sigma}_r^{(+1r)}+\bar{\sigma}_r^{(+1,+1)}}{2}\right) - \frac{\bar{\sigma}_\theta^{(+1r)}+\bar{\sigma}_\theta^{(+1,+1)}}{2r}, & (r,z)\in\gamma_3,\\ \frac{1}{r}\bar{r}\left(\bar{\sigma}_{rz}\right)_z - \frac{1}{r}\frac{2}{h_1}\bar{r}\left(\frac{\bar{\sigma}_r+\bar{\sigma}_r^{(+1z)}}{2}\right) - \frac{\bar{\sigma}_\theta+\bar{\sigma}_\theta^{(+1z)}}{2r}, & (r,z)\in\gamma_4,\\ \frac{1}{r}\frac{2}{h_1}\bar{r}^{(+1)}\bar{\sigma}_r^{(+1,+1)} + \frac{1}{r}\frac{2}{h_2}\bar{r}^{(+1)}\bar{\sigma}_{rz}^{(+1,+1)} - \frac{\bar{\sigma}_\theta^{(+1,+1)}}{r}, & (r,z)\in\gamma_{13},\\ \frac{1}{r}\frac{2}{h_1}\bar{r}^{(+1)}\bar{\sigma}_r^{(+1r)} - \frac{1}{r}\frac{2}{h_2}\bar{r}^{(+1)}\bar{\sigma}_{rz}^{(+1r)} - \frac{\bar{\sigma}_\theta^{(+1r)}}{r}, & (r,z)\in\gamma_{23},\\ -\frac{1}{r}\frac{2}{h_1}\bar{r}\bar{\sigma}_r^{(+1z)} + \frac{1}{r}\frac{2}{h_2}\bar{r}\bar{\sigma}_{rz}^{(+1z)} - \frac{\bar{\sigma}_\theta^{(+1z)}}{r}, & (r,z)\in\gamma_{14},\\ -\frac{1}{r}\frac{2}{h_1}\bar{r}\bar{\sigma}_r - \frac{1}{r}\frac{2}{h_2}\bar{r}\bar{\sigma}_{rz} - \frac{\bar{\sigma}_\theta}{r}, & (r,z)\in\gamma_{24}, \end{cases}$$

$$\Lambda_2(y,g,\mu)=\begin{cases}\frac{1}{r}\left(\bar{r}\frac{\bar{\sigma}_{rz}+\bar{\sigma}_{rz}^{(+1_z)}}{2}\right)_r+\frac{1}{r}\left(\frac{\bar{r}\bar{\sigma}_z+\bar{r}^{(+1)}\bar{\sigma}_z^{(+1_r)}}{2}\right)_z, & (r,z)\in\omega_h,\\ \frac{1}{r}\left(\bar{r}\bar{\sigma}_{rz}^{(+1_z)}\right)_r+\frac{1}{r}\frac{2}{h_2}\left(\frac{\bar{r}\bar{\sigma}_z^{(+1_z)}+\bar{r}^{(+1)}\bar{\sigma}_z^{(+1,+1)}}{2}\right), & (r,z)\in\gamma_1,\\ \frac{1}{r}\left(\bar{r}\bar{\sigma}_{rz}\right)_r-\frac{1}{r}\frac{2}{h_2}\left(\frac{\bar{r}\bar{\sigma}_z+\bar{r}^{(+1)}\bar{\sigma}_z^{(+1_r)}}{2}\right), & (r,z)\in\gamma_2,\\ \frac{1}{r}\bar{r}^{(+1)}\left(\bar{\sigma}_z^{(+1_r)}\right)_z+\frac{1}{r}\frac{2}{h_1}\bar{r}^{(+1)}\left(\frac{\bar{\sigma}_{rz}^{(+1_r)}+\bar{\sigma}_{rz}^{(+1,+1)}}{2}\right), & (r,z)\in\gamma_3,\\ \frac{1}{r}\bar{r}\left(\bar{\sigma}_z\right)_z-\frac{1}{r}\frac{2}{h_1}\bar{r}\left(\frac{\bar{\sigma}_{rz}+\bar{\sigma}_{rz}^{(+1_z)}}{2}\right), & (r,z)\in\gamma_4,\\ \frac{1}{r}\frac{2}{h_2}\bar{r}^{(+1)}\bar{\sigma}_z^{(+1,+1)}+\frac{1}{r}\frac{2}{h_1}\bar{r}^{(+1)}\bar{\sigma}_{rz}^{(+1,+1)}, & (r,z)\in\gamma_{13},\\ \frac{1}{r}\frac{2}{h_1}\bar{r}^{(+1)}\bar{\sigma}_{rz}^{(+1_r)}-\frac{1}{r}\frac{2}{h_2}\bar{r}^{(+1)}\bar{\sigma}_z^{(+1_r)}, & (r,z)\in\gamma_{23},\\ -\frac{1}{r}\frac{2}{h_1}\bar{r}\bar{\sigma}_{rz}^{(+1_z)}+\frac{1}{r}\frac{2}{h_2}\bar{r}\bar{\sigma}_z^{(+1_z)}, & (r,z)\in\gamma_{14},\\ -\frac{1}{r}\frac{2}{h_1}\bar{r}\bar{\sigma}_{rz}-\frac{1}{r}\frac{2}{h_2}\bar{r}\bar{\sigma}_z, & (r,z)\in\gamma_{24},\end{cases}$$

$$\Lambda_3(y,g,\mu)=\begin{cases}\frac{1}{r}\left(\bar{r}\frac{\bar{D}_r+\bar{D}_r^{(+1_z)}}{2}\right)_r+\frac{1}{r}\left(\frac{\bar{r}\bar{D}_z+\bar{r}^{(+1)}\bar{D}_z^{(+1_r)}}{2}\right)_z, & (r,z)\in\omega_h,\\ \frac{1}{r}\left(\bar{r}\bar{D}_r^{(+1_z)}\right)_r+\frac{1}{r}\frac{2}{h_2}\left(\frac{\bar{r}\bar{D}_z^{(+1_z)}+\bar{r}^{(+1)}\bar{D}_z^{(+1,+1)}}{2}\right), & (r,z)\in\gamma_1,\\ \frac{1}{r}\left(\bar{r}\bar{D}_r\right)_r-\frac{1}{r}\frac{2}{h_2}\left(\frac{\bar{r}\bar{D}_z+\bar{r}^{(+1)}\bar{D}_z^{(+1_r)}}{2}\right), & (r,z)\in\gamma_2,\\ \mu, & (r,z)\in\bar{\omega}_h/(\omega_h\cup\gamma_1\cup\gamma_2),\end{cases}$$

$$F_3=\begin{cases}f_3, & (r,z)\in\omega_h\cup\gamma_1\cup\gamma_2,\\ 0 & (r,z)\in\bar{\omega}_h/(\omega_h\cup\gamma_1\cup\gamma_2),\end{cases}$$

$$F_1=f_1+\begin{cases}0, & (r,z)\in\omega_h,\\ -\frac{2}{h_2}p_{rt}^{(0)}, & (r,z)\in\gamma_1,\\ \frac{2}{h_2}p_{rt}^{(1)}, & (r,z)\in\gamma_2,\\ -\frac{2}{h_1}p_r^{(0)}, & (r,z)\in\gamma_3,\\ \frac{2}{h_1}p_r^{(1)}, & (r,z)\in\gamma_4,\\ -\frac{2}{h_1}p_r^{(0)}-\frac{2}{h_2}p_{rt}^{(0)}, & (r,z)\in\gamma_{13},\\ -\frac{2}{h_1}p_r^{(0)}+\frac{2}{h_2}p_{rt}^{(1)}, & (r,z)\in\gamma_{23},\\ \frac{2}{h_1}p_r^{(1)}-\frac{2}{h_2}p_{rt}^{(0)}, & (r,z)\in\gamma_{14},\\ \frac{2}{h_1}p_r^{(1)}+\frac{2}{h_2}p_{rt}^{(1)}, & (r,z)\in\gamma_{24},\end{cases}\qquad F_2=f_2+\begin{cases}0, & (r,z)\in\omega_h,\\ -\frac{2}{h_2}p_z^{(0)}, & (r,z)\in\gamma_1,\\ \frac{2}{h_2}p_z^{(1)}, & (r,z)\in\gamma_2,\\ -\frac{2}{h_1}p_{zt}^{(0)}, & (r,z)\in\gamma_3,\\ \frac{2}{h_1}p_{zt}^{(1)}, & (r,z)\in\gamma_4,\\ -\frac{2}{h_1}p_{zt}^{(0)}-\frac{2}{h_2}p_z^{(0)}, & (r,z)\in\gamma_{13},\\ -\frac{2}{h_1}p_{zt}^{(0)}+\frac{2}{h_2}p_z^{(1)}, & (r,z)\in\gamma_{23},\\ \frac{2}{h_1}p_{zt}^{(1)}-\frac{2}{h_2}p_z^{(0)}, & (r,z)\in\gamma_{14},\\ \frac{2}{h_1}p_{zt}^{(1)}+\frac{2}{h_2}p_z^{(1)}, & (r,z)\in\gamma_{24}.\end{cases}$$

References

[1] A. Ballato, Piezoelectricity: old effect, new thrusts, IEEE Trans. Ultrason., Ferroelect. 42 (5) (1995) 916.
[2] D.A. Berlincourt, D.R. Curran, H. Jaffe, Piezoelectric and piezomagnetic materials and their function in transducers, in: W.P. Mason (Ed.), Physical Acoustics, vol. 1A, Academic Press, New York, 1964, pp. 204–236.
[3] G.R. Buchanan, J. Peddieson Jr., Vibration of infinite piezoelectric cylinders with anisotropic properties using cylindrical finite elements, IEEE Trans. Ultrason., Ferroelect., Freq. Contr. 38 (3) (1991) 291–301.
[4] R.C. Buchanan, Ceramic Materials for Electronics: Processing, Properties and Applications, Marcel Dekker, New York, 1991.
[5] E.F. Crawley, Intelligent structures for aerospace: a technology overview and assessment, AIAA J. 32 1689–1699.
[6] E. Dieulesaint, D. Royer, Elastic Waves in Solids: Applications to Signal Processing, Wiley, Chichester, 1980.
[7] J.T. Fielding et al., Characterization of PZT hollow-sphere transducers, Proceedings of the IX IEEE International Symposium on Applications of Ferroelectrics, 1994, pp. 202–205.
[8] E. Fukada, Poiseuille medal award lecture: Piezoelectricity of biopolymers, Biorheology 32 (1995) 593.
[9] X. Geng, Q.M. Zhang, Evaluation of piezocomposites for ultrasonic transducer applications – influence of the unit cell dimensions and the properties of constituents on the performance of 2–2 piezocomposites, IEEE Trans. Ultrason., Ferroelect., Freq. Contr. 44 (4) (1997) 857–872.
[10] T.R. Gururaja, Piezoelectric transducers for medical ultrasonic imaging, Amer. Ceramic Soc. Bull. 73 (5) (1994) 50–55.
[11] T. Ikeda, Fundamentals of Piezoelectricity, Oxford University Press, Oxford, 1990.
[12] Y. Kagawa, T. Tsuchiya, T. Kawashima, Finite element simulation of piezoelectric vibrator gyroscopes, IEEE Trans. Ultrason., Ferroelect., Freq. Contr. 43 (4) (1996) 509–520.
[13] Y. Kagawa, T. Tsuchiya, G. Furukawa, Finite element simulation of dynamic responces of piezoelectric actuators, J. Sound Vibration 191 (4) (1996) 519–528.
[14] J.S. Lee, Boundary element method for electroelastic interaction in piezoceramics, Engrg. Anal. Boundary Elements 15 (4) (1995) 321–328.
[15] R. Le Letty, F. Claeyssen, R. Bossut, Combined finite element-normal mode expansion methods in electroelasticity and their application to piezoactive motors, Int. J. Numer. Methods Engrg. 40 (18) (1997) 3385–3395.
[16] R. Lerch, Simulation of piezoelectric devices by two- and three-dimensional finite elements, IEEE Trans. Ultrason., Ferroelect., Freq. Contr. 37 (3) (1990) 233–243.
[17] Y.C. Liang, C. Hwu, Electromechanical analysis of defects in piezoelectric materials, Smart Mater. Struct. 5 (1996) 314–320.
[18] P. Lu, O. Mahrenholtz, A variational boundary element formulation for piezoelectricity, Mech. Res. Commun. 21 (6) (1994) 605–615.
[19] R.V.N. Melnik, M.N. Moskalkov, Difference schemes for and analysis of approximate solutions of two-dimensional nonstationary problems in coupled electroelasticity, Differential Equations, vol. 27, No. 7, 1991, pp. 1220–1230 (Plenum Press/Consultants Bureau, New York, 1992, pp. 860–867).
[20] R.V.N. Melnik, The stability condition and energy estimate for non-stationary problems of coupled electroelasticity, Math. Mech. Solids 2 (2) (1997) 153–180.
[21] R.V.N. Melnik, K.N. Melnik, A note on the class of weakly coupled problems of non-stationary piezoelectricity, Commun. Numer. Methods Engrg. 14 (1998) 839–847.
[22] R.V.N. Melnik, Generalised solutions, discrete models, and energy estimates for a 2D problem of coupled field theory, Appl. Math. Comput. 107 (1999) 27–55.
[23] R.V.N. Melnik, K.N. Melnik, Courant–Friederichs–Lewy type stability conditions in two-dimensional dynamic electroelasticity, TR Series, Faculty of Sciences, Department of Mathematics & Computing, University of Southern Queensland, SC-MC-9707, 1997, submitted.
[24] A.A. Samarskii, Theorie der Differenzenverfahren, (Series: Mathematik und ihre Anwendungen in Physik und Technik), Aufl. Leipzig: Academische Verlagsgesellschaft Geest & Portig, 1984.
[25] A.A. Samarskii, E.S. Nikolaev, Numerical Methods for Grid Equations, Birkhauser, Basel, 1989.
[26] N. Turbe, G.A. Maugin, On the linear piezoelectricity of composite materials, Math. Methods Appl. Sci. 14 (1991) 403–412.
[27] A.O. Vatulyan, V.L. Kublikov, Boundary element method in electroelasticity, Boundary Elements Commun. 6 (2) (1995) 59–61.